JOURNAL OF GEOPHYSICAL RESEARCH: OCEANS, VOL. 118, 5703–5719, doi:10.1002/jgrc.20413, 2013

Surges around the Hawaiian Islands from the 2011 Tohoku Tsunami

Kwok Fai Cheung,[1] Yefei Bai,[1] and Yoshiki Yamazaki[1]

Received 6 June 2013; revised 19 August 2013; accepted 22 September 2013; published 22 October 2013.

[1] The 2011 Tohoku tsunami devastated the northeastern Japan coasts and caused localized damage to coastal infrastructure across the Pacific. The tsunami resulted in strong currents around the Hawaiian Islands that led to closure of harbors and marinas for up to 38 h after its arrival. We utilize a nonhydrostatic model to reconstruct the tsunami event from the seismic source for elucidation of the physical processes and inference of the coastal hazards. A number of tide gauges, bottom pressure sensors, and ADCPs provided point measurements for validation and assessment of the model results in Hawaii. Spectral analysis of the computed surface elevation and current reveals complex flow patterns due to multiscale resonance. Standing waves with 33–75 min period develop along the island chains, while oscillations of 27 min or shorter are primarily confined to an island or an island group with interconnected shelves. Standing edge waves with periods 16 min or shorter, which are able to form nodes on the reefs and inside harbors, are the main driving force of the observed coastal currents. Resonance and constructive interference of the oscillation modes provide an explanation of the impacts observed in Hawaii with implications for emergency management in Pacific island communities.

Citation: Cheung, K. F., Y. Bai, and Y. Yamazaki (2013), Surges around the Hawaiian Islands from the 2011 Tohoku Tsunami, *J. Geophys. Res. Oceans*, *118*, 5703–5719, doi:10.1002/jgrc.20413.

1. Introduction

[2] The Tohoku earthquake of M_w 9.0 ruptured the megathrust fault offshore of northeastern Honshu on 11 March 2011 and generated a devastating near-field tsunami with 39.75 m of runup [*Mori et al.*, 2011]. The Pacific Tsunami Warning Center issued a warning for Hawaii at 9:31 P.M. 10 March local time, prompting state-wide evacuation of coastal residents and marine vessels. The waves reached Hawaii at 3:00 A.M. on the following day, 7 h after the earthquake, and caused localized damage and inundation across the state. The Pacific Tsunami Warning Center canceled the warning for Hawaii at 7:31 A.M., when the wave amplitude had reduced to less than 1 m at tide gauges around the islands. The advisory remained in effect until 11:26 A.M., when the instrument readings fell below 0.5 m. The Hawaiian Islands, however, are prone to trapping of tsunami energy [*Munger and Cheung*, 2008]. Their steep volcanic slopes results in small footprints on the abyssal seafloor with limited damping to large-scale resonance oscillations. The surges continued unabated for another day with hazardous currents at harbors and beaches. The shallow reef and shelf systems along Hawaii's coastlines might also play a role in the enduring surges and localized impacts as observed on Tutuila during the 2009 Samoa tsunami [*Roeber et al.*, 2010b].

[3] The US Coast Guard (USCG) logs provide a proxy to assess the resonance in Hawaii waters from the 2011 Tohoku tsunami. Kauai experienced the least impact with moderate surges along the coasts despite its exposed location to the tsunami (see Figure 1 for location maps). After a brief inspection, USCG reopened Nawiliwili Harbor and Port Allen at 10:00 and 10:27 A.M. on 11 March local time. This was followed by Honolulu Harbor on Oahu at 10:38 A.M. The adjacent Keehi Lagoon, however, experienced strong currents at 15 min period. USCG deployed a vessel outside the entrance to prevent evacuated boaters from returning until 5:31 P.M. on 12 March. Hilo Harbor experienced a mix of 15 and 30 min oscillations and together with Kawaihae Harbor also on Hawaii Island remained closed until 2:19 P.M. on 11 March. Maui, Molokai, and Lanai, which are situated on interconnected insular shelves known collectively as Maui Nui, experienced energetic wave activities along their coastlines. Kahului Harbor saw the largest wave that inundated its facilities 2 h after the first and lingering 0.3–0.9 m oscillations at 15 min period well into the afternoon. The surges were strong enough to empty Maalaea Harbor at 75 min intervals 10 h after the tsunami arrived. When both facilities were reopened at 4:22 P.M. on 11 March, surges of 1.2–1.5 m at 25 min intervals still prevailed at nearby Lahaina Harbor, which remained closed until 9:07 A.M. on 12 March. Such persistent and localized oscillations were also observed at harbors across the Pacific Ocean in the aftermath of the tsunami [*Allan et al.*, 2012; *Lynett et al.*, 2013].

Additional supporting information may be found in the online version of this article.

[1]Department of Ocean and Resource Engineering, University of Hawaii at Manoa, Honolulu, Hawaii, USA.

Corresponding author: K. F. Cheung, Department of Ocean and Resource Engineering, University of Hawaii at Manoa, Honolulu, HI 96822, USA. (cheung@hawaii.edu)

2169-9275/13/10.1002/jgrc.20413

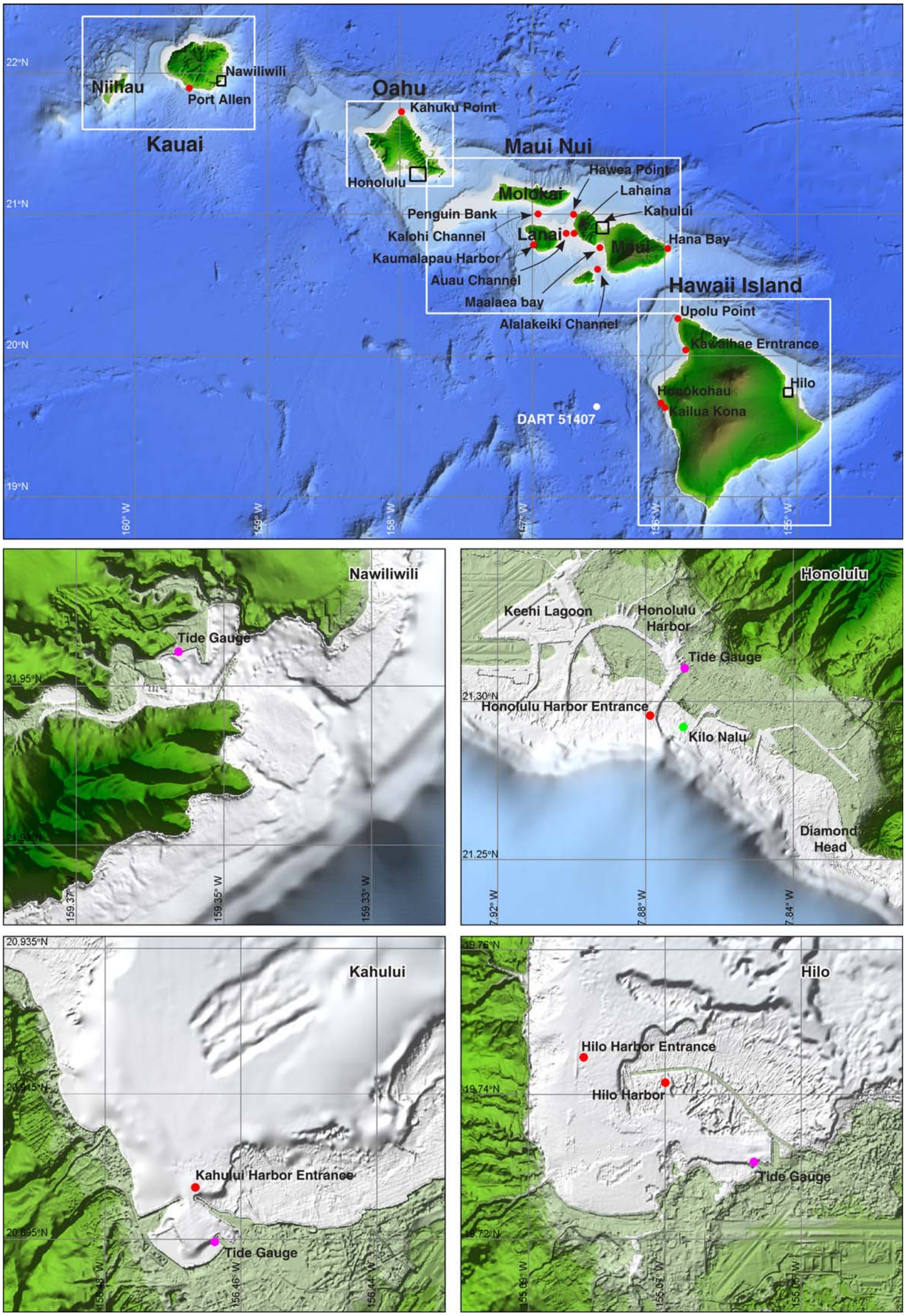

Figure 1. Location and relief maps for Hawaii and the four major commercial harbors of the state. Purple, green, red, and white circles indicate tide gauges, Kilo Nalu ADCP and pressure sensor, NOAA ADCPs, and DART buoys. White rectangles in the top panel are outlines of level-3 computational grids.

[4] Numerical modeling of the 2011 Tohoku tsunami allows reconstruction of the wave conditions for elucidation of the physical processes [*Grilli et al*., 2013; *Wei et al*., 2013; *Yamazaki et al*., 2011b]. In particular, *Yamazaki et al*. [2011b] modeled the tsunami in the near field from finite-fault inversion of seismic waves and reproduced nearshore buoy measurements along the east and north Japan coasts. *Yamazaki et al*. [2012] subsequently validated the model data with DART measurements around the North Pacific and provided preliminary results of the surges along the Honolulu coast. The present study extends their spectral analysis of the computed surface elevation to cover all major islands and commercial harbors of Hawaii and provides an overall assessment of the resonance behaviors and localized impacts associated with the tsunami. The results for the Honolulu coast are recomputed over a larger region that covers the entire reef system of interest. Figure 1 shows the locations of tide gauges, bottom pressure sensors, and the Kilo Nalu ADCP (Acoustic Doppler Current Profiler) operated by the University of Hawaii that recorded clear signals of the tsunami for validation of the model results. In addition, 18 ADCPs deployed by NOAA in major waterways and near harbor entrances around Hawaii fortuitously recorded currents from the tsunami. Despite having large sampling intervals of 6 min, the instruments provided good coverage of the impacted locations during the event. Given the handful of tsunami current records in the literature [*Bricker et al*., 2007; *Lacy et al*., 2012; *Sobarzo et al*., 2012], the NOAA ADCP data set deserves a serious investigation of its relevance and implications for tsunami research.

2. Tsunami Modeling

[5] We utilize NEOWAVE (Non-hydrostatic Evolution of Ocean Wave) to model the 2011 Tohoku tsunami from its generation by the earthquake rupture to the surge conditions along Hawaii's coastlines. The staggered finite-difference model builds on the nonlinear shallow-water equations with a vertical velocity term to account for weakly dispersive waves and a momentum conservation scheme to describe flow discontinuities [*Yamazaki et al*., 2009, 2011a]. The vertical velocity term also facilitates modeling of tsunami generation and transfer of kinetic energy from seafloor deformation. This dynamic source mechanism complements the nonhydrostatic formulation to provide accurate descriptions of the near and far-field wave dynamics [*Yamazaki et al*., 2012, 2013]. The Hawaiian Islands are exposed peaks of seamounts originated from volcanic activities and shaped by massive landslides. Coral reefs cover 70% of the coastlines in the subtropical environment [*Battista et al*., 2007]. As illustrated in Figure 1, the nearshore bathymetry is characterized by shallow reef flats with abrupt drop off to an insular shelf surround by steep slopes. NEOWAVE can describe the vertical flow structure over steep bathymetry and shock-related hydraulic processes such as tsunami bores or hydraulic jumps that might develop in the shallow-reef environment [*Roeber et al*., 2010a; *Roeber and Cheung*, 2012].

[6] The model utilizes up to five levels of two-way nested grids to capture physical processes with increasing resolution from the open ocean to Hawaii's coastlines. The bathymetry and topography come from ETOPO1, multibeam, and LiDAR data at 1 arcmin (~1800 m), 50 m, and 1–3 m resolution. Hydrographic surveys and digitized nautical charts supplement the nearshore bathymetry, mostly inside harbors and marinas, where the water lacks clarity for LiDAR surveys. The Generic Mapping Tools (GMT) of *Wessel and Smith* [1991] blends the data sets for development of the computational grids. The level-1 grid extends from (15°N, 225°W) to (62°N, 150°W) at 2 arcmin (~3600 m) resolution to model propagation of the tsunami across the Northern Pacific, while the level-2 grid captures the wave transformation along the Hawaiian Island chain from (18.5°N, 160.8°W) to (22.6°N, 154.2°W) at higher resolution of 24 arcsec (~720 m). As outlined in Figure 1, the level-3 grids cover Kauai, Oahu, and Maui Nui at 3 arcsec (~90 m) and Hawaii Island at 6 arcsec (~180 m). An intermediate level of grids brings the resolution of Hawaii Island's coasts to 3 arcsec (~90 m). The finest grids at levels 4 or 5 cover 7 to 11 km of coastlines and resolve the reefs, channels, and shores around the instrument locations at 0.3 arcsec (~9 m). A Manning coefficient of 0.035 describes the subgrid roughness for the nearshore reefs and the volcanic substrates of Hawaii [*Bretschneider et al*., 1986].

[7] The tsunami source is defined by the finite-fault model, P-MOD2 with strike angle of 192°, which is based on inversion of seismic waves recorded around the world and iterative forward modeling of tsunami waveforms at near-field buoys off the Japan coasts [*Yamazaki et al*., 2011b]. *Lay et al*. [2011] provided a detailed description of the model comprising a 380 × 200 km^2 fault plane with 190 subfaults of 20 × 20 km^2 each and an epicenter at (38.107°N, 142.916°E). The schematized rupture, which begins at 19.5 km beneath of the continental slope, propagates radially with an initial velocity of 1.5 km/s out to a distance of 100 km and 2.5 km/s beyond that. The faulting lasts for 150 s and produces 62 m of near-trench slip consistent with geodetic records from *Ito et al*. [2011] and *Simons et al*. [2011]. The finite-fault model resolves the slip time histories of the individual subfaults to collectively match the recorded seismic waves. Implementation of the planar fault model of *Okada* [1985] defines the elastic crustal deformation associated with the slip at each subfault. The method of superposition reconstructs the time history of ground motions from the finite-fault model and defines the input for dynamic modeling of tsunami generation in NEOWAVE.

[8] The computation covers 13 h of elapsed time to capture the resonance oscillations around the Hawaiian Islands during the crucial initial hours of the event. The tsunami arrived at Honolulu Harbor when the tide was 0.13 m below MSL (mean sea level). Since the tide range is only 0.3 m in Hawaii, the use of MSL in the computation should not noticeably affect the results at the instrument locations, which are in harbors and channels of over 11 m deep. The still-water initial condition ignores tidal currents, which are typically too weak to modify tsunami propagation around the Hawaiian Islands, but might be strong enough to influence inundation around large estuaries and rivers on continental coasts [*Zhang et al*., 2011]. The time step varies from 1 s at the level-1 computational grid to 0.05 s at the finest grids at level-4 or level-5. The

output intervals of the model results are 30 s over the computational grids to resolve the oscillations in the frequency domain through spectral analysis. The computed surface elevation and flow velocity are interpolated at the instrument locations for comparison with recorded data at 60 s intervals.

3. Comparison With Recorded Data

[9] The 2011 Tohoku tsunami produced instrumentally recorded data sets of unprecedented quality and coverage for model validation and scientific research. The NEOWAVE results have given good agreement with measurements from 16 DART buoys in the North Pacific [*Yamazaki et al*., 2012]. A number of tide gauges, bottom pressure sensors, and ADCPs recorded surface elevation and current data for assessment of the model results across Hawaii (see Figure 1 for location maps). The nearshore circulation driven by winds, waves, eddies, and tides are known to be complex in the strongly stratified water around Hawaii [e.g., *Eich et al*., 2004; *Lowe et al*., 2009; *Johnson et al*., 2013]. The ADCP measurements show variations of the flow velocity over the water column before the tsunami arrived indicative of three-dimensional background currents. We computed the depth-averaged velocity, which is most relevant to the primary flow caused by tsunamis, from the arithmetic mean of the recorded components over the water column in the north-south and east-west directions. The surface elevation and depth-averaged velocity components were then processed through a Butterworth high-pass filter to remove tidal and other background signals with periods longer than 3 h. The DART and tide-gauge data at 60 s intervals does not require filtering of signals associated with wind-generated waves. The Kilo Nalu surface elevation and flow velocity, which were recorded at a high sampling rate of every 2 s, were processed through a low-pass filter to remove signals with periods shorter than 60 s.

[10] The computed time series have been shifted by 6 min for comparison with the measurements. This accounts for underestimation of travel time by the model due to the lack of secondary dispersion effects associated with earth elasticity and water density variation [*Tsai et al*., 2013]. NEOWAVE well reproduces the amplitude, period, and phase of the surface elevation measurements in Figure 2a. Since resonance results in persistent surges after the initial tsunami waves, the computed amplitude spectrum by Fast Fourier Transform (FFT) provides good indication of the dominant oscillation modes at each location. The time series and spectral signals vary along the island chain. As shown in *Yamazaki et al*. [2012], DART 51407 at 50 km west of Hawaii Island recorded strong signals at 43 and 75 min period. Shorter components with decreasing amplitude over time are likely due to higher-harmonic release from scattering of the initial waves and subsequent arrival of dispersive waves. The Nawiliwili tide gauge on Kauai also recorded the 43 and 75 min components albeit with stronger signals of 20 min and shorter. The two long-period modes are overshadowed by resonance oscillations around 30 min at Hilo and Kahului. The water level at Kahului fell below the range of the tide gauge during the first two waves and peaked at 2.07 m during the fourth. The Honolulu tide gauge and Kilo Nalu pressure sensor recorded strong 43 min signals with a broadband extending to longer periods. The tsunami waveform at Kilo Nalu on an open coast shows distinguishable signals as short as 5 min period. All the water-level stations show long-period oscillations between 100 and 200 min associated with large-scale standing edge waves along the continental margin off Japan [*Yamazaki et al*., 2013].

[11] The Kilo Nalu ADCP recorded currents atop a fringing reef at 12.2 m water depth and 400 m offshore. Figure 2b shows good agreement between the computed and recorded data despite the complexity of tsunami processes over the shelf and reef system. The signals include harmonic components down to 3 min period overlapping with the infragravity band of wind-generated waves. NEOWAVE reproduces the waveform and spectral content of the dominant flow in the north-south direction. The background current, which is evident in the east-west direction prior to tsunami arrival, is likely responsible for the spectral peaks around 60 and 100 min period not recorded at other locations. The waves between 5 and 16 min periods have comparable or greater contributions to the currents at Kilo Nalu albeit with much weaker surface signals in comparison to the 43 min component. The computed short-period waves deviate from the measurements over time due to difficulties in capturing dispersion and scattering across the Pacific with the 2 arcmin level-1 grid. The NOAA ADCPs provided additional measurements of coastal currents for examination of the modeled results. Figure 3 compares the velocity components in the north-south and east-west directions at instruments around Oahu, Kauai, and Hawaii Island. NEOWAVE provides similar results at the Honolulu ADCP located at 15 m water depth 990 m west of Kilo Nalu. The recorded data at 6 min intervals shows long-period components such as the 43 min peak, but fails to produce signals below the 12 min Nyquist period.

[12] The Kahuku ADCP at 68.1 m water depth on the north shore of Oahu and the Port Allen ADCP at 12.5 m water depth on the south shore of Kauai recorded strong background signals before the tsunami arrived. Their large recording intervals could not register tsunami signals below 12 min periods that were abundant over the shelves and reefs as inferred from the model results. Similar issues arise with the data recorded at Upolu, Kawaihae, Honokohau, and Kona on the west side of Hawaii Island. In particular, the Honokohau and Kona ADCPs at 42.6 and 27.5 m water depth could not detect the dominant tsunami signals below 12 min. The harmonic components between 30 and 75 min, which dominate the surface elevation signals, have minor contributions to the currents over the narrow shelves along the coast. The background currents appear to be weaker over the insular shelf on the east side of Hawaii Island. The ADCP at the Hilo Harbor entrance recorded the 30 min resonance mode of the embayment. Attenuation of short-period oscillations across the 1050 m wide and 19 m deep entrance results in better agreement of the measurements and model results. The ADCP inside the harbor recorded additional signals above 12 min period associated with oscillations in the semienclosed basin. The model data reproduces the recorded signals reasonably well even with shorter period surges expected of the ADCP location on a shallow reef.

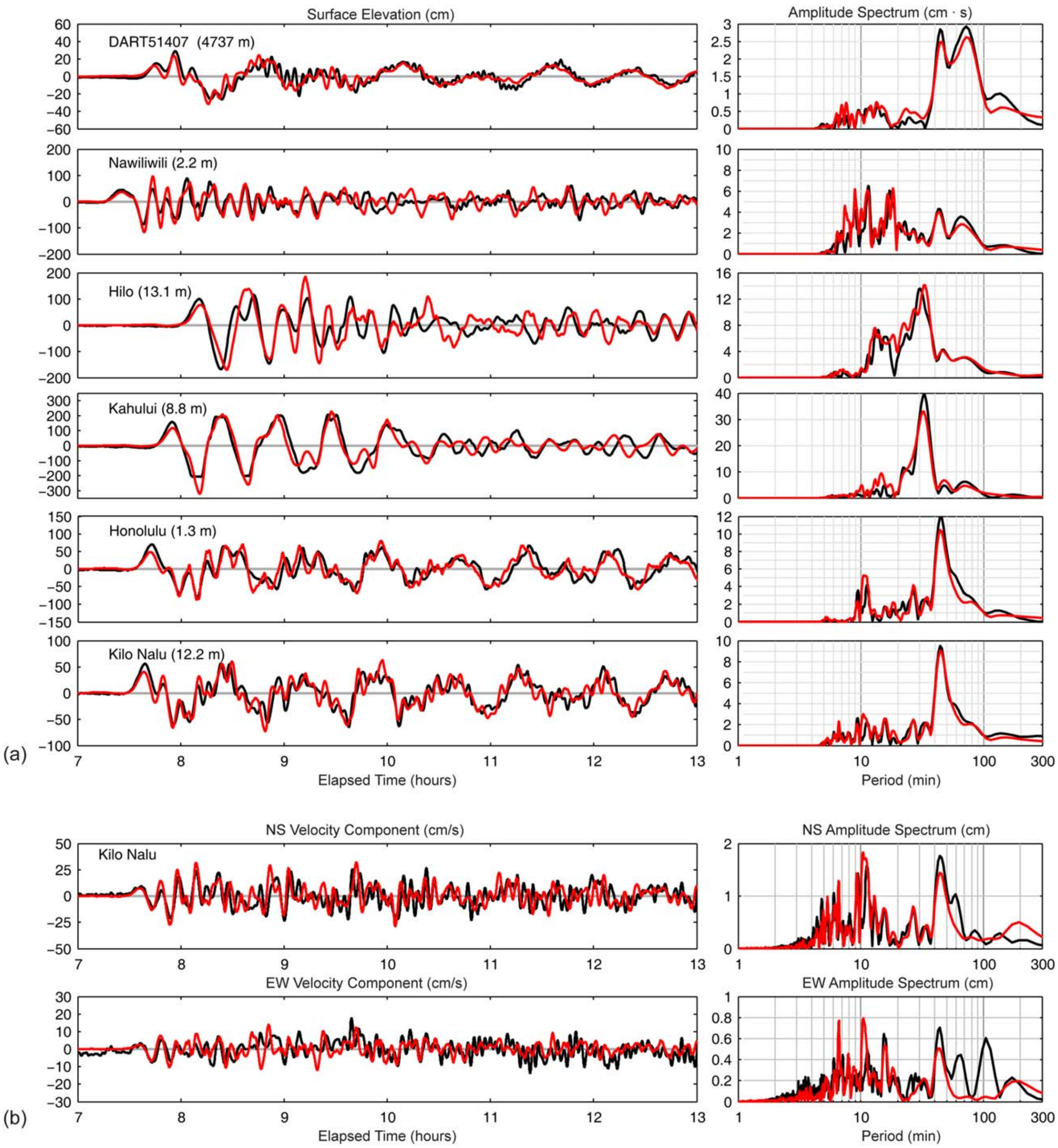

Figure 2. Comparison of computed (red) and recorded (black) data for model validation: (a) surface elevation at tides gauges and Kilo Nalu pressure sensor and (b) depth-averaged current velocity at Kilo Nalu ADCP. The water depth at the instrument location is in parentheses after the label. The computed time series have been shifted forward by 6 min to account for early arrival of the modeled tsunami. Kilo Nalu is the only location with concurrent surface elevation and current measurements. The waves between 5 and 16 min period have greater contributions to the current albeit with much weaker surface signals in comparison to the 43 min dominant component.

[13] The tsunami exhibits a range of patterns over the interconnected insular shelves around Maui. Figure 4 compares the computed and recorded velocity components at the NOAA ADCPs over Maui Nui, except for the one in Kaumalapau Harbor due to the lack of high-resolution LiDAR bathymetry around Lanai. The computed and recorded data at the Kalohi, Auau, and Alalakeiki ADCPs, which were located in the interisland channels at 106.2, 73.5, and 156.5 m water depth, show good agreement due to dominance of the signals between 27 and 75 min periods. Oscillations below 12 min are relatively weak at these midchannel locations, but become more noticeable near the shore at the

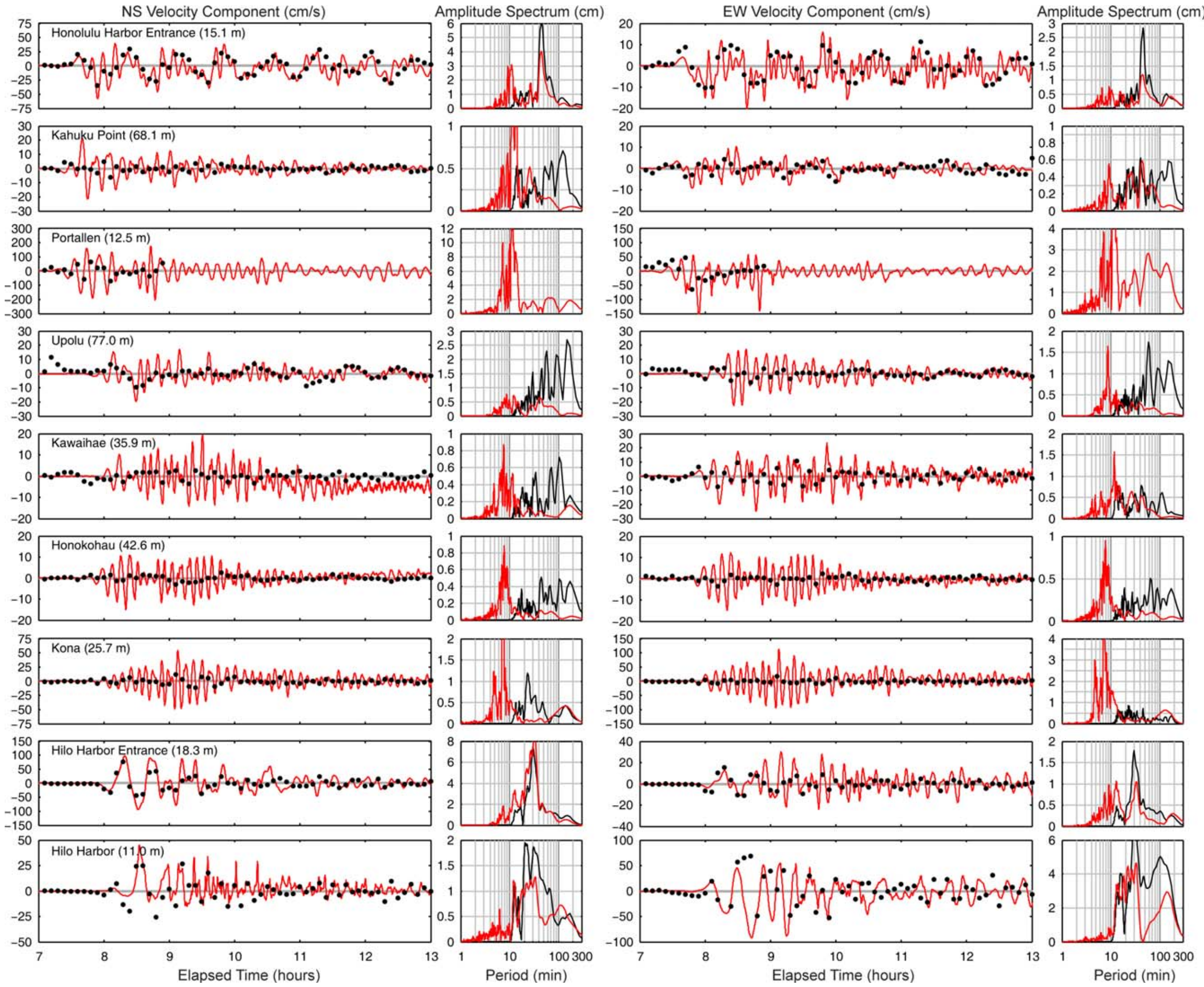

Figure 3. Comparison of computed (red) and recorded (black) depth-averaged current velocity at NOAA ADCPs around Oahu, Kauai, and Hawaii Island. The water depth at the instrument location is in parentheses after the label. The computed time series have been shifted forward by 6 min to account for early arrival of the modeled tsunami. The ADCPs cannot fully capture the coastal currents because of large recording intervals of 6 min.

Hawea, Maalaea, and Lahaina ADCPs. The long-period components from 27 to 75 min diminish at the Hana ADCP, which was located at 21.1 m water depth on a narrow insular shelf. The model data shows dominance of 4–12 min oscillations over the reef and shelf complex that were completely omitted by the 6 min sampling interval of the measurements. The recorded 20 min peak is likely due to background currents visible in the time series prior to arrival of the tsunami. The Kakului ADCP, which was located at 14.3 m water depth just outside the harbor entrance, recorded signals with a dominant 33 min peak associated with resonance of the embayment. Despite the presence of short-period nearshore oscillations and long-period background signals, the ADCP measurements and model data show reasonable agreement due to the strong 33 min signals.

4. Multiscale Resonance

[14] The 2011 Tohoku tsunami had dominant periods of 45, 60, and 90 min associated with the rupture and secondary components between 30 and 234 min emitted from trapped waves along northeast Japan coasts [*Yamazaki et al*., 2013]. The incident, scattered, and dispersive waves could trigger a wide range of oscillations along the Hawaiian Islands. Tsunami signals are nonstationary and most suitable for wavelet analysis [*Bricker et al*., 2007]. However, observations and measurements have indicated occurrences of persistent, periodic surges after the transient initial waves. The analysis of surface elevations at tide gauges and pressure sensors has already demonstrated the use of an FFT algorithm to determine the amplitude spectrum over wave period and identify dominant oscillation modes along the island chain. Implementation of the same algorithm at all grid points defines the spatial distributions of the spectral amplitude and phase angle for visualization of the oscillation modes. The time series must have the same starting point and step size to retain coherent spatial structures across grid points and levels. Better frequency resolution can be achieved by extending the time series

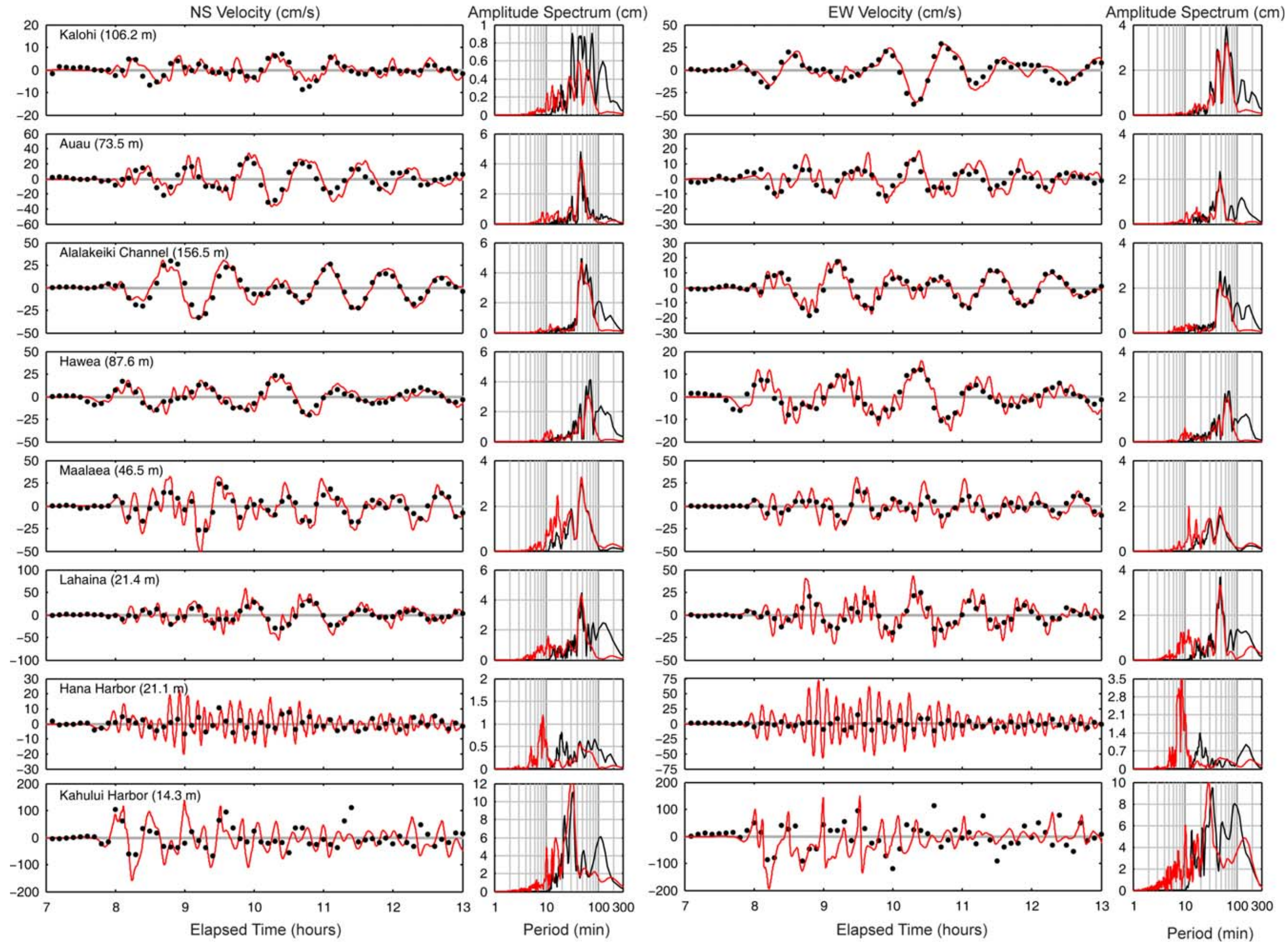

Figure 4. Comparison of computed (red) and recorded (black) depth-averaged current velocity at NOAA ADCP around Maui Nui. The water depth at the instrument location is in parentheses after the label. The computed time series have been shifted forward by 6 min to account for early arrival of the modeled tsunami. The ADCPs cannot fully capture the coastal currents because of large recording intervals of 6 min.

with zero entries until the total number of steps reaches the next integer power of 2. A Hanning window reduces the effects of the finite-length time series, but the resulting Fourier coefficients must be rescaled to account for energy loss [*Emery and Thompson*, 2001]. Since FFT is a linear process, the swash zone is excluded from the analysis and the nonlinear time-domain solution is denoted by a series of oscillation modes in the frequency domain.

[15] The spectral analysis of the computed surface elevation shows identifiable oscillation modes from 3 min in the infragravity range to 110 min at the interisland scale. Figure 5 plots the spectral amplitude of four oscillation modes from 33 to 75 min that extend along the island chain with high energy. These interisland modes have large bandwidths as indicated by the respective spectral peaks in Figure 2. The transition from one mode to the next is distinct owing to the discrete wavelengths that can span across the interisland channels. The 100 m depth contour indicates the approximate extent of the insular shelf for reference. The phase angle plots in Figure S1 of the supporting information assist interpretation of the oscillation modes. Standing and partial standing waves associated with resonance have distinct nodal lines, where the amplitude is nearly zero and the phase varies rapidly across by 180°. The spectral analysis can be extended to the computed flow velocity by including a directional component in the FFT algorithm [*Emery and Thompson*, 2001]. This will introduce an additional dimension to the amplitude spectrum that might complicate interpretation of the results. A simple relation can help infer the current pattern from the surface amplitude. The wave amplitude and flow speed have a 90° phase difference typical of standing waves in which the strongest horizontal flow occurs at the nodal lines and the water is nearly stagnant at the antinodes. Progressive waves, on the other hand, have continuous phase variations and relatively uniform amplitude and speed in space.

[16] The oscillation mode at 75 min extends 2400 km along the archipelago from Hawaii Island to Midway in the northwest. The interisland standing waves have strong local amplification over Maui Nui and a well defined nodal line to the southwest of Oahu (see Figure 1 for location maps). The water from Oahu to Hawaii Island forms an antinode that oscillates with the same phase over the abyssal plain. At 52 min period, the antinode splits into a standing wave with a node across Maui. The local shelf amplification develops into a separate standing wave system with a node

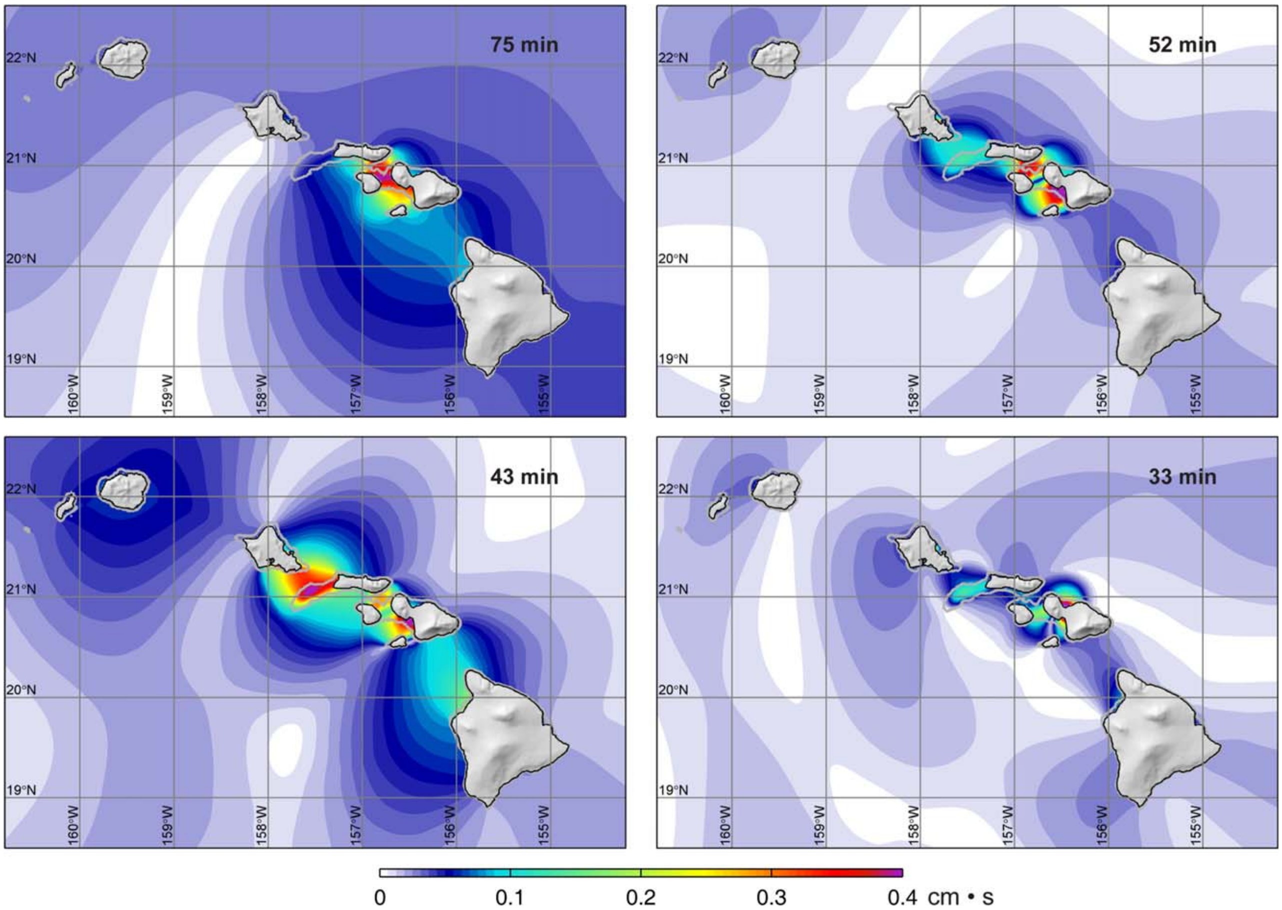

Figure 5. Spectral amplitude of surface-elevation time series around the Hawaiian Islands. Gray lines are 100 m depth contours delineating the approximate extent of insular shelves.

at Auau Channel and an antinode at Maalaea Bay that coincides with the node of the interisland system obscuring its features. The interisland standing waves are much better defined in the 43 min mode with nodes at west Oahu, east Maui, and east Hawaii Island, while the high-energy system over the shelves develops new nodes at south Molokai and south Maui. The two systems of standing waves are coupled and are in phase at Penguin Bank, where the large-amplitude oscillation controls the resonance across the island chain. DART 51407 recorded strong signals at 43 and 75 min and the data off the Honolulu coasts shows a broadband 43 min peak extending to the 52 min mode because of their locations in the respective antinodes. The 33 min mode is a transition when the interisland standing waves weaken and oscillations over the insular shelf gain dominance. A system of standing waves extends from Penguin Bank through the interisland channels to northwest Hawaii Island. This oscillation mode, which culminates at Kahului Bay and saturates the tide gauge signals, is responsible for the inundation of harbor facilities during the event.

[17] Island-scale oscillation modes are primarily confined to an island or in an island group with interconnected shelves. The transition from one mode to the next is smooth as the rugged coastline and varying shelf produce infinite combinations of eigenmodes. Figure 6 and Figure S2 of the supporting information show selected oscillation modes around Hawaii Island, where insular shelves exist primarily on the north-facing shores. The 30 min mode still has influence from interisland standing waves across Maui Nui. The oscillation at the northwest shore extends to Maui with the same phase and to the rest of the island through well-defined nodal lines. A key feature is the resonance of Hilo Bay with a nodal line that couples the embayment, island-scale, and interisland oscillations. Such multiscale resonance is a common occurrence during tsunami events [*Horrillo et al*., 2008; *Yamazaki and Cheung*, 2011; *Bellotti et al*., 2012]. The 27 min mode, which is primarily confined to Hawaii Island, is dominated by the wide embayment on the northwest shore. The dominant oscillation shifts to the narrower northeast shelf at 21 min period. As the period decreases from 30 to 21 min, the resonance oscillation in Hilo Bay contracts into the harbor with the nodal line migrated to the entrance. Mode-0 standing edge waves develop on the northeast shore at 14 min period. The dispersion relation of *Ursell* [1952] reproduces the wavelength of 78 km with an average slope of 0.07 from the coastline to the 450 m depth contour, which corresponds to the approximate offshore extent of the edge waves. The system has an antinode in Hilo Bay that in turn couples with the harbor oscillation. As the period decreases from 21 to 14 min, the nodal line rotates from the entrance to the center of the basin giving rise to a sloshing mode. The Hilo Harbor ADCP recorded strong signals of these oscillation modes because

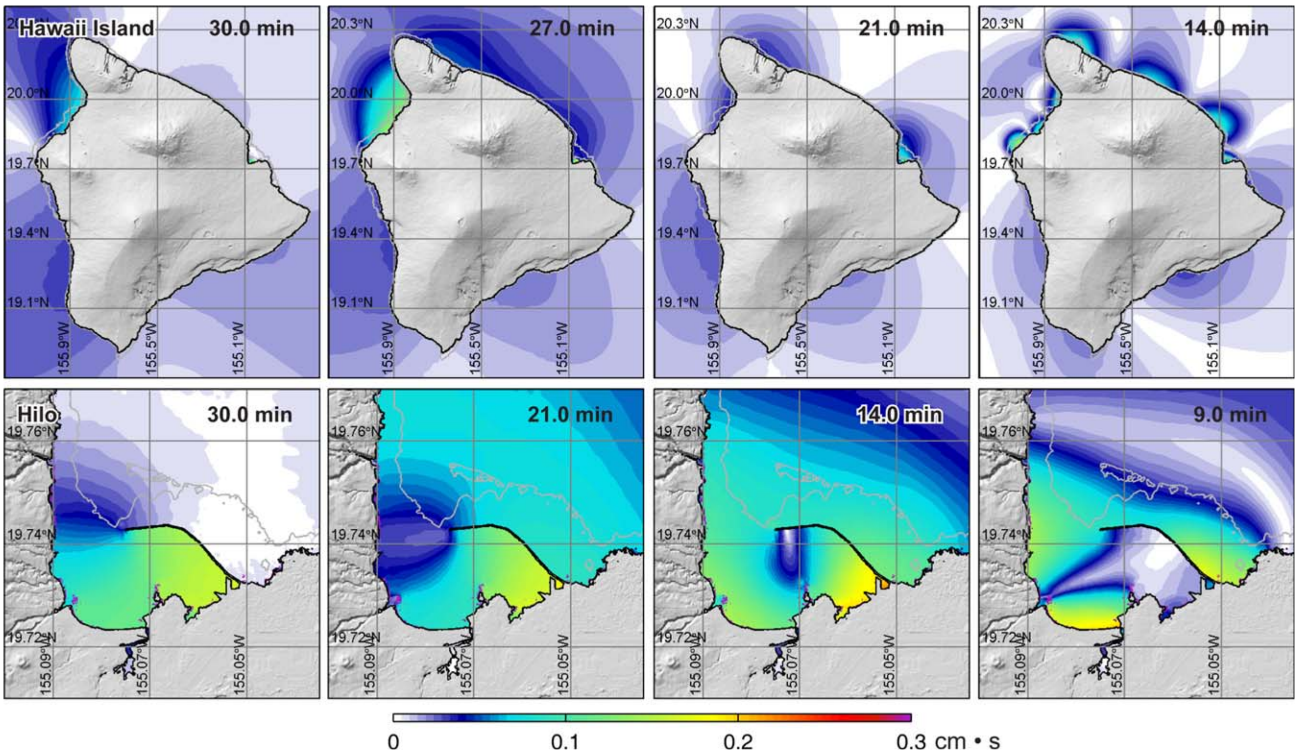

Figure 6. Spectral amplitude of surface-elevation time series around Hawaii Island and Hilo. Gray lines are 20 and 100 m depth contours delineating the approximate extents of nearshore reefs in Hilo Bay and insular shelves around Hawaii Island.

of its location adjacent to the node. At 9 min period, the standing edge wave extends into Hilo Bay with a nodal line at the fore reefs just outside the 20 m depth contour. The ship basin behind the breakwater turns into a node that extends across the harbor. The tide gauge did not register signals from this mode because of its location at the node.

[18] The wide shelves and extensive reefs give rise to complex wave patterns around Oahu. Figure 7 and Figure S3 of the supporting information show selected oscillation modes for illustration. The 22.5 min mode features a standing wave over the wide concave shelf on the north shore of Oahu. The standing wave is coupled with the oscillations on the east and south shores through a well-defined node at the northeast headland. Mode-0 standing edge waves develop on the north shore at 15 min period, while the oscillations on the east and south shores show a combination of amplification and resonance over the reefs delineated by the 20 m depth contour. The 14 min mode shows three antinodes on the north shore and development of nodal lines at the reefs around the island. On the Honolulu coast, well-defined nodes develop at the entrances to Honolulu Harbor and Keehi Lagoon at 16 min period. The shorter wavelength at 13 min shifts the node from the harbor entrance into the basin and creates additional nodes inside Keehi Lagoon. The 10.5 min mode indicates considerable oscillations in the inner reef region and formation of nodes at both entrances to Honolulu Harbor. The reefs and dredged basins play a significant role in the coastal currents during tsunamis. Standing waves with 16 min period or shorter are able to develop nodes on the reefs providing an explanation for the currents recorded by the Kilo Nalu ADCP despite the relatively weak surface signatures. Although the model only shows moderate surface oscillations in Keehi Lagoon, strong currents associated with the nodal lines likely damaged boats and dock facilities and prevented boaters from returning for 2 days.

[19] The proximity of Kauai and Niihau plays a significant role in the resonance characteristics. Figure 8 and Figure S4 of the supporting information show dominant oscillation modes around the two islands and Nawiliwili Harbor. The first mode at 23 min period corresponds to resonance of the shelves between the two islands with local amplification over the wide insular shelf on northwest Kauai. At 20.5 min period, the local amplification turns into a standing wave that couples with the interisland oscillation with a nodal line. Standing edge waves become dominant over the insular shelves at 14 min period. The interisland standing waves form a nodal line across the channel to couple the shelf oscillations between the two islands. The lack of prominent reef structures enables formation of mode-0 standing edge waves with periods as low as 6.5 min over the insular shelves. The resulting nodes account for the strong oscillatory currents between 6 and 14 min period at Port Allen as shown in Figure 3. Nawiliwili Harbor, which is in an estuary sheltered by a breakwater, experiences large-amplitude oscillations at 18.5 min period. The lack of a nodal line or rapid phase transition indicates local amplification of the estuary from island-scale standing waves. Resonance of the harbor occurs at 11.5 min with a well-defined node at the entrance. The nodal line rotates and shifts inward as the period decreases leading to formation of sloshing modes between 9 and 6.5

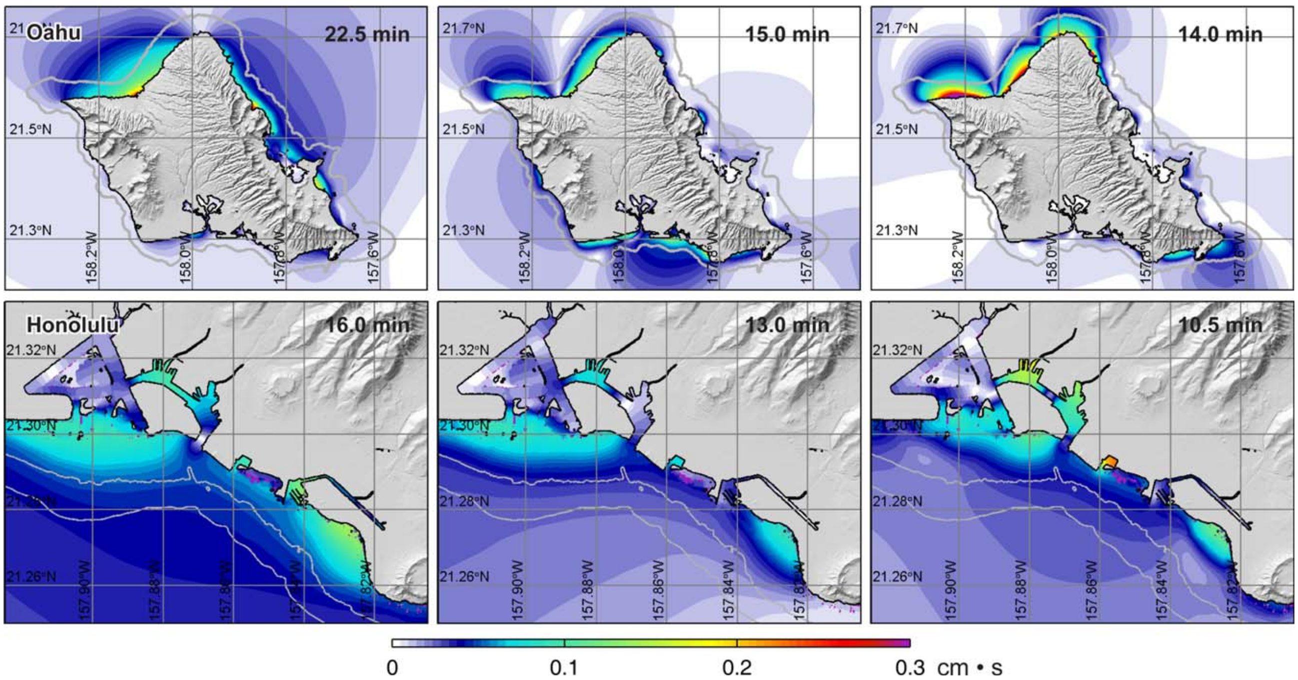

Figure 7. Spectral amplitude of surface-elevation time series around Oahu and Honolulu. Gray lines are 20 (Honolulu only) and 100 m depth contours delineating the approximate extents of nearshore reefs and insular shelves.

min in the basin. The Nawiliwili tide gauge was well positioned to record signals at and below 18.5 min period during the event.

[20] The interconnected insular shelves and shallow channels of Maui Nui produce unique oscillation modes dominated by Penguin Bank. The 32 km long and 16 km wide feature with relatively uniform water depth of approximately 50 m and steep flanks is effective in trapping tsunami waves below the interisland range. Figure 9 and Figure S5 of the supporting information show the oscillation modes enumerated by the standing waves over the open shelf. The first and second modes at 27 and 24 min show one and two antinodes over Penguin Bank that are coupled with the standing waves extending along the interisland channels to Kahului and Maalaea. The third mode at 20.5 min shows oscillations with three antinodes over Penguin Bank that are out-of-phase or decoupled from the standing waves along the channels and shelves. Standing and progressive edge waves with periods 17.5 min or shorter become dominant around Maui. To accommodate the decreasing wavelength, the oscillations over Penguin Bank turn into a transverse mode at 16 min and a combined transverse and longitudinal mode at 12.5 min or shorter. Standing edge waves below 12.5 min period do not have sufficient energy at the channel centerlines, where the Kalohi, Auau, and Alalakeiki ADCPs are located, providing an explanation for the decent records of the tsunami even with large sampling intervals of 6 min. The computed signals at the Kawea Point, Lahaina, and Maalaea ADCPs reflect the increasing influences of these edge waves closer to the shore. The high-energy oscillations are primarily within the insular shelves delineated by the 100 m depth contour. At Hana, the lack of wave activities above 12 min period is due to the narrow insular shelf and steep slope that favor shorter period waves as indicated by the computed results at the ADCP in Figure 4.

[21] The surges at Kahului Harbor, which is located at the head of a V-shape bay protected by two breakwaters, are dominated by the 33 min interisland mode. The island-scale oscillations from 16 to 27 min also contribute to local spectral peaks of the recorded surface elevation and velocity components. Figure 10 and Figure S6 of the supporting information show oscillation modes at 16 min and shorter that are active in the inner bay, where fringing reefs extend about 2 km offshore on either side of the harbor. The 16 min mode shows an offshore nodal point and local amplification over the reefs and in the harbor. The gradual phase variation around the node indicates progressive edge waves that propagate in a circular pattern within the V-shape bay. The 14 min amplitude plot indicates standing waves over the reefs with nodal lines along the edges. The offshore nodal point returns at 12 min period but the progressive edge waves in the bay are accompanied by out-of-phase oscillations over the reefs and in the harbor. A nodal line develops just outside the harbor entrance indicating resonance of the basin. At 7 min period, additional nodal lines develop between the two breakwaters and along the fringing reefs inside the harbor. The well-defined nodal lines indicate the reef, harbor, and shelf oscillations are coupled with a 180° phase shift across each body of water. Because of the large areas and the narrow opening between the breakwaters, these oscillation modes can produce significant perturbations of the currents at the harbor entrance despite their weak surface signals.

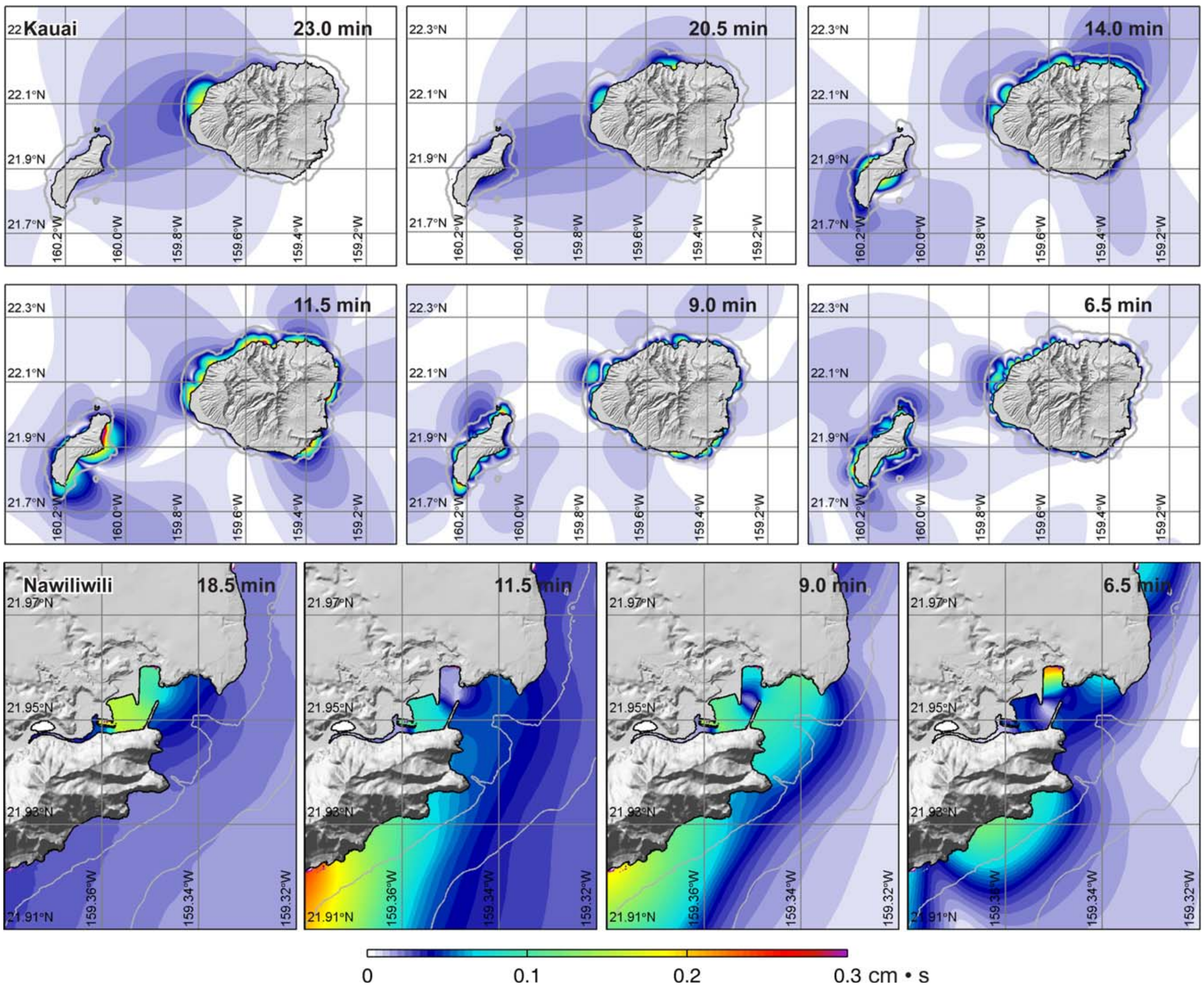

Figure 8. Spectral amplitude of surface-elevation time series around Kauai and Nawiliwili. Gray lines are 20 (Nawiliwili only) and 100 m depth contours delineating the approximate extents of nearshore reefs and insular shelves.

5. Tsunami Surges

[22] The resonance modes and the spectral signatures of the incoming waves are the main driving factors for the localized impacts observed in Hawaii. Model results of the 2011 Tohoku tsunami show long-period resonance modes at 52 and 75 min that are not evident in the 2006 Kuril Islands tsunami [*Munger and Cheung*, 2008]. The combination of these two modes centered at Maui Nui with the 33 and 43 min interisland modes resulted in the inundation at Kahului Harbor and the emptying of Maalaea Harbor well after the tsunami had arrived. Constructive interference of resonance modes at the coast is a common occurrence during tsunami events [*González et al*., 1995; *Yamazaki and Cheung*, 2011; *Yamazaki et al*., 2013]. Island-scale oscillation modes at 27 min and below dominate the wave activities over the insular shelves. Standing waves with periods 16 min or shorter can amplify or resonate over the reefs to produce locally strong currents. These multiscale oscillation modes provide an alternate view of the wave dynamics and coastal impacts, even though some of them might be coupled nonlinearly or phased-locked to reflect transient processes in the computed time series. Figure 11 illustrates the combined effects of the oscillation modes by plotting the maximum surface elevation and depth-averaged flow speed at the four islands or island groups. Heightened wave activities are primarily within the insular shelves delineated by the 100 m depth contour. The tsunami amplitude off the insular shelf is typically less than 0.5 m and the flow speed is negligible.

[23] Standing edge waves give rise to the primary surges around Niihau, Kauai, and Oahu. Despite the direction of the tsunami from the northwest, the surface elevation is larger on the wider insular shelf of southeast Niihau. The influence of the edge-wave modes is most prominent on Oahu's north shore, where some of the highest runup from the tsunami was recorded in Hawaii. The surface elevation shows a general proportional relation with the shelf width as seen on continental coasts [*Yamazaki and Cheung*,

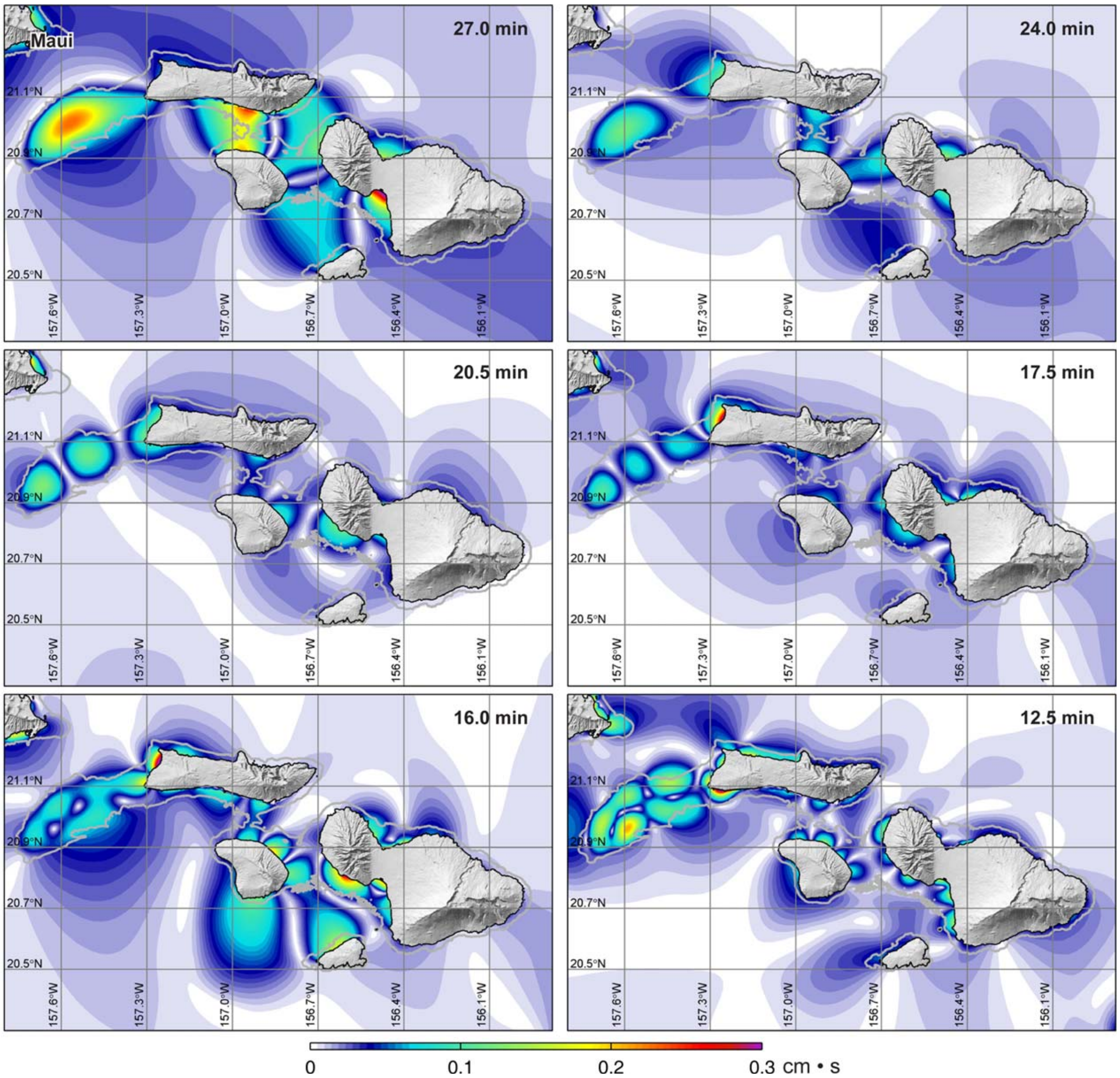

Figure 9. Spectral amplitude of surface-elevation time series around Maui Nui. Gray lines are 100 m depth contours delineating the approximate extent of insular shelves.

2011]. The flow speed, however, does not always have a direct relation with the surface elevation. The east and south shores of Oahu have moderate wave amplitude, but show consistently strong currents due to development of coupled oscillations over the shelves and reefs. Flow speeds of 1 m/s or higher typically occur over the fringing reefs extending 1–2 km from the shore. Maui Nui has relatively uniform surface elevation around 1 m associated with the interisland modes over Penguin Bank and in the channels. The island-scale standing waves augment the oscillation amplitude over the insular shelves. The current is weak in the channels reaching only 0.3 m/s at nodal lines of the resonance modes, but strengthens to 1 m/s or higher over the prominent reef systems on the south shore of Molokai and in Kahului and Maalaea Bays. The north-facing shores of Hawaii Island can sustain standing edge waves on the insular shelves and broadband resonance modes in Hilo Bay. The southern half of the island primarily exhibits amplification of large-scale oscillations on the concave coastlines. The currents are negligible in the absence of insular shelves.

[24] Tsunami surges are a major concern for harbor masters and the US Coast Guard. Figure 12 plots the maximum surface elevation and depth-average flow speed at Honolulu, Nawiliwili, Hilo, and Kahului Harbors from model results of the 2011 Tohoku tsunami. The Kilo Nalu records show the 43 min interisland mode dominates the background surge with approximately 0.5 m elevation off the Honolulu coasts. The long-period oscillations give rise to gentle flood and ebb flows over the shelf and reef system [*Yamazaki et al.*, 2012]. Local amplification and resonance of shorter period waves augment the surface elevation to at least 1.5 m at several locations. The currents result from standing edge waves with periods 16 min or shorter. Their nodes define the nearshore flow pattern with speeds as high as 3.3 m/s at entrance channels to dredged basins. While

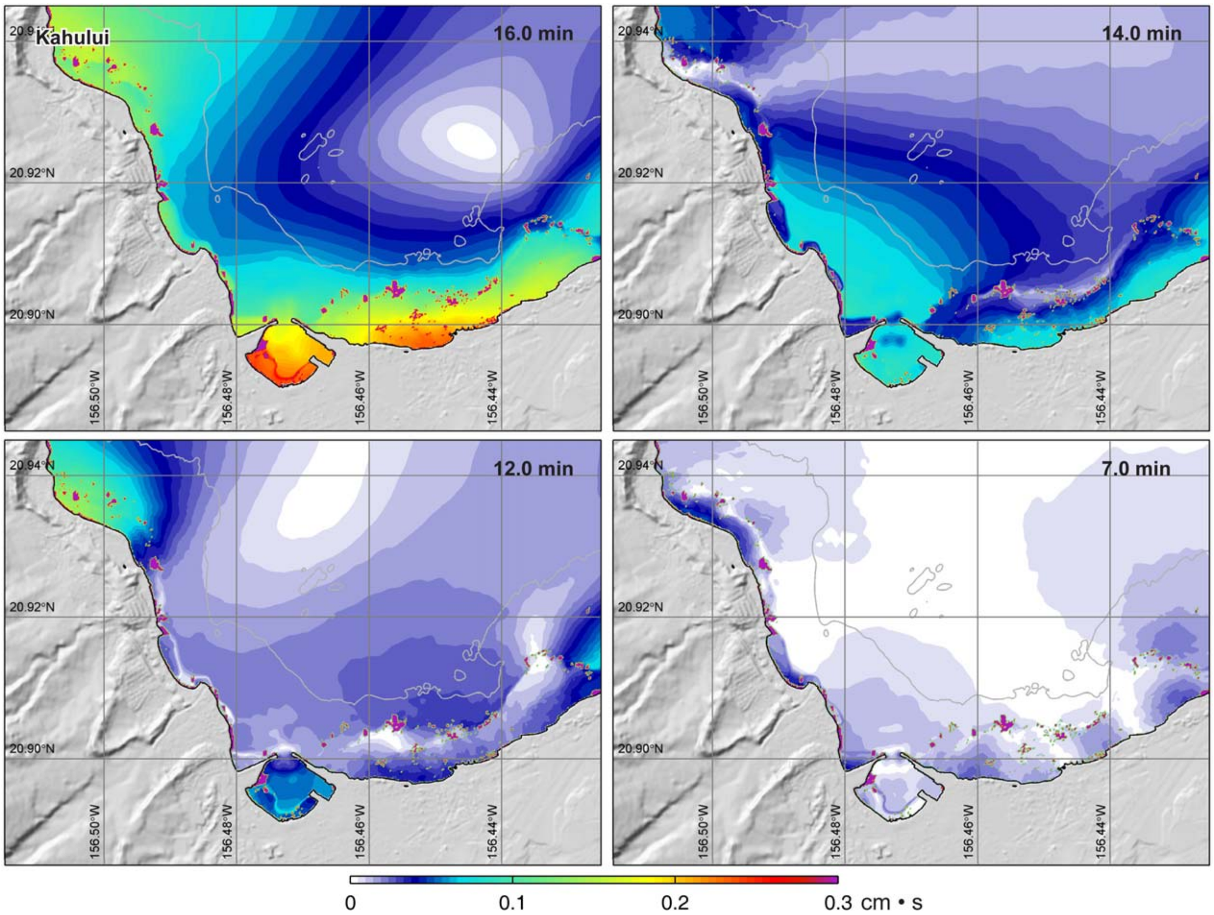

Figure 10. Spectral amplitude of surface-elevation time series around Kahului. Gray lines are 20 m depth contours delineating the approximate extent of nearshore reefs.

the surface signal is weak in Keehi Lagoon, the current reaches over 1.5 m/s in the marina area adjacent to Honolulu Harbor. Nawiliwili Harbor on Kauai is located in a river estuary semienclosed by a breakwater. The interisland modes, which are apparent outside the 100 m contour, account for less than 0.2 m of surface elevation. The island-scale oscillations below 20 min period increase the surface elevation to 1.2 m inside the harbor. The surface depression and the strong local current of 4 m/s at the breakwater head are due to intersection of nodal lines at the harbor entrance from oscillation modes between 6.5 and 11.5 min. For both Honolulu and Nawiliwili, the current typically drops below 0.5 m/s outside the 20 m depth contour delineating the approximate extent of the reefs.

[25] The surges in Hilo and Kahului Harbors are strongly influenced by the respective embayments. The surface elevation of around 0.5 m at the mouth of Hilo Bay is representative of the interisland modes. Resonance oscillations between 9 and 30 min period give rise to 1.5 m of surface elevation over the reefs and 2.1 m at the shore inside the harbor. The surface elevation plot shows a depression at the breakwater head, where nodal lines of the 14–21 min modes originate. The combination of these oscillation modes produces strong currents of 3.5 m/s over the reefs. The well-defined nodal line of the 9 min mode gives rise to 2.8 m/s of currents on the west side of the harbor basin. At Kahului Bay, the interisland modes account for as much as 0.75 m of surface elevation at the 100 m contour near its mouth. The dominant 33 min interisland mode increases its amplitude rapidly into the bay and along with the island-scale oscillations at and below 27 min augment the surface elevation to 2.5 m over the fringing reefs inside and outside the harbor. The V-shape embayment focuses the flow to around 0.7 m/s at the 20 m contour. The reefs amplify the currents to over 3 m/s along their edges, which coincide with the nodal lines of the 14, 12, and 7 min modes. The flow speeds up as it passes through the harbor entrance resulting in strong currents of 6 m/s. The NOAA ADCP located at a small offset from the harbor entrance in 14.3 m of water recorded the ingress and egress with a dominant period of 33 min. As shown in Figure 4, the measurements provide validation of the model data in the complex current field adjacent to the strong outflow jet.

[26] Resonance modes and periods are intrinsic to the landform and independent of the excitation. The interisland modes at 33 and 43 min and the island-scale oscillations for Oahu are similar to those obtained by *Munger and Cheung* [2008] using a nonlinear shallow-water model, but the periods are off by up to 1.5 min. The present nonhydrostatic approach, which includes a vertical velocity term, can resolve the flow structure over the steep insular slopes and their abrupt transition to the shelves. Although tsunamis are shallow-water waves, dispersion over the insular slopes can modify the wavelength-period relation and consequently the

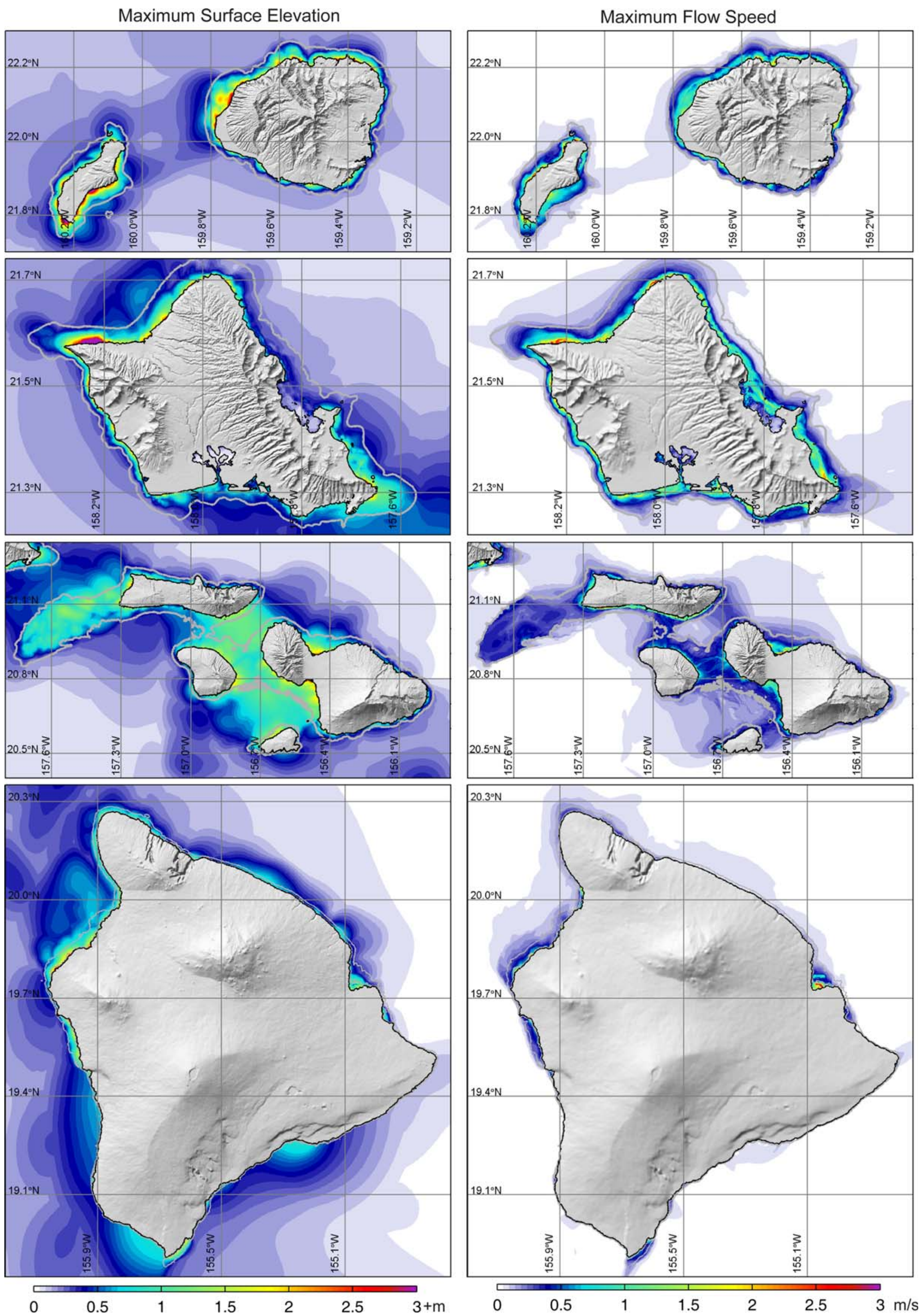

Figure 11. Maximum surface elevation and flow speed around the major Hawaiian Islands. Gray lines are 100 m depth contours delineating the approximate extent of insular shelves.

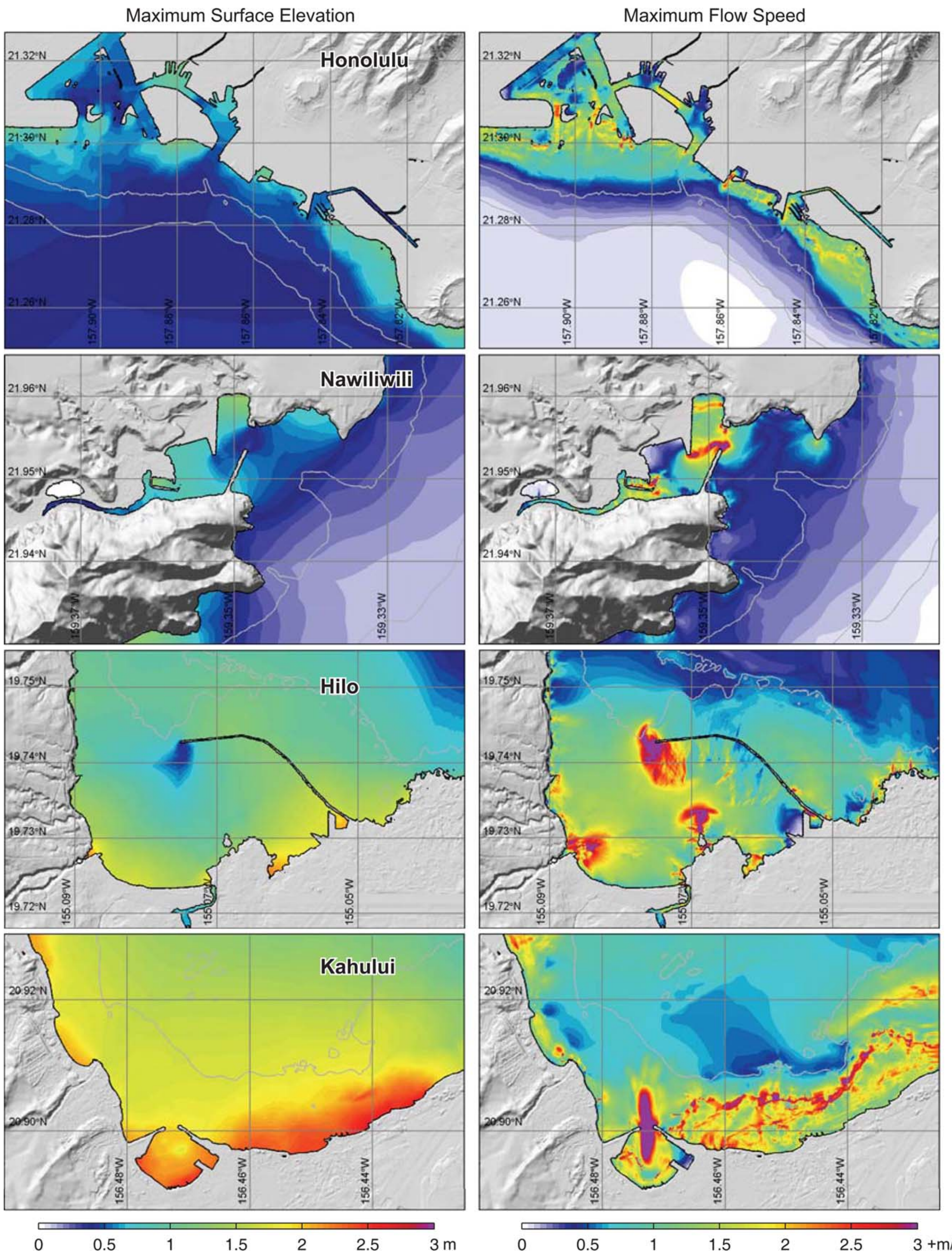

Figure 12. Maximum surface elevation and flow speed at the four major commercial harbors of Hawaii. Gray lines are 20 and 100 m (if present) depth contours delineating the approximate extent of nearshore reefs and insular shelves.

resonance modes and periods along the island chain. A nonhydrostatic model such as NEOWAVE can better describe the amplitude, phase, and period of oscillation modes for mapping and assessment of tsunami hazards in volcanic island environments. The island-scale and interisland resonance periods are in the typical range of tsunami energy, indicating the susceptibility of the shallow shelves and embayments to oscillations. The regions with large wave amplitude from the 2011 Tohoku tsunami have been sites of damaging inundation in prior tsunamis from Kamchatka, Alaska, and Chile as documented by *Walker* [2004]. The resonance modes allow identification of areas susceptible to flood hazards and strong currents for development of response and mitigation plans by emergency management agencies in Hawaii.

6. Conclusions

[27] The 2011 Tohoku tsunami caused persistent oscillations and hazardous currents in coastal waters around Hawaii that resulted in damage and lengthy closure of harbors and marinas. The nonhydrostatic model NEOWAVE is able to reconstruct the tsunami from its generation by a finite-fault solution to the surge conditions along Hawaii's coastlines. Prior validation with DART data has confirmed the model results across the North Pacific. Tide gauges in major commercial harbors across Hawaii and an ADCP and a pressure sensor operated by the University of Hawaii off the Honolulu coast provide the most pertinent data set to validate the computed surface elevation and current in tropical, volcanic island environments. The model results also corroborate current measurements from a number of NOAA ADCPs in shipping channels and harbor entrances during the event. The 6 min sampling interval, however, cannot capture short-period surges on the reefs that saturate the signals recorded by the University of Hawaii instruments.

[28] The validated model data provides a wealth of information for studies of tsunami processes in Hawaii. With proper preprocessing, Fast Fourier Transform is able to resolve the spectral contents of tsunami signals as well as their spatial structures. The nonlinear evolution of the surface elevation is denoted by a series of oscillation modes in the frequency domain. The results provide an alternate view of the wave dynamics and coastal impacts that would otherwise not be obvious in the time domain. The oscillation modes are classified as interisland and island scale that can be attributed, respectively, to the archipelago and the slope and shelf system of each island or island group. The distinct nodes and antinodes indicate formation of standing waves and trapping of tsunami energy. Penguin Bank, which is a 32 km long and 16 km wide shelf of approximately 50 m deep, dominates a range of oscillation modes stretching from Oahu to Hawaii Island. The multiscale oscillations play an important role in the observed and recorded surge conditions.

[29] The interisland oscillation modes from 33 to 75 min period produce strong and distinct surface signals across Hawaii. Standing edge waves with periods 27 min and below are active over the insular slopes and shelves. The tsunami wave amplitude does not provide a direct indication of the coastal current. The interisland standing waves dominate the surface elevation with their large amplitude and bandwidth, but only produce gentle flood and ebb flows over the shelves. Standing waves with periods 16 min or shorter are able to form a series of nodes on the reefs that result in strong local currents despite their weak surface signature. Tide gauge data are therefore insufficient for use as a proxy to determine beach and harbor safety after a tsunami event. Since the island-scale resonance modes have low damping, their coupling with the reef oscillations results in enduring surges along the coast. NEOWAVE, which is able to describe the inherent processes, provides a tool to delineate safe zones for marine vessels and identify at-risk localities in a tsunami event.

[30] **Acknowledgments.** This work was funded in part by the National Tsunami Hazard Mitigation Program grant NA09NWS4670016 through Hawaii State Civil Defense. Thorne Lay of University of California Santa Cruz and Geno Pawlak of University of California San Diego are the original sources of the fault-fault solution and the Kilo Nalu measurements. The tsunami warning timelines, DART buoy measurements, and tide gauge and ADCP records reside on www.ptwc.weather.gov, www.ndbc.noaa.gov, and www.tidesandcurrents.noaa.gov. We would like to thank Joanna Nunan of the US Coast Guard Fourteenth District for the logs and observations of the 2011 Tohoku tsunami in Hawaii as well as Giorgio Bellotti, two anonymous reviewers, and the Associate Editor for their comments and suggestions that have improved this paper. SOEST contribution 8979.

References

Allan, J. C., P. D. Komar, P. Ruggiero, and R. Witter (2012), The March 2011 Tohoku tsunami and its impacts along the U.S. west coast, *J. Coastal Res.*, *28*(5), 1142–1153.

Battista, T. A., B. M. Costa, and S. M. Anderson (2007), Shallow-water benthic habitats of the Main Eight Hawaiian Islands (DVD), *NOAA Tech. Memo. NOS NCCOS 61*, Biogeography Branch, Silver Spring, Md.

Bellotti, G., R. Briganti, and G. M. Beltrami (2012), The combined role of bay and shelf modes in tsunami amplification along the coast, *J. Geophys. Res.*, *117*, C08027, doi:10.1029/2012JC008061.

Bretschneider, C. L., H. J. Krock, E. Nakazaki, and F. M. Casciano (1986), Roughness of typical Hawaiian terrain for tsunami run-up calculations: A user's manual, J.K.K. Look Lab. Rep., Univ. of Hawaii, Honolulu.

Bricker, J. D., S. Munger, C. Pequignet, J. R. Wells, G. Pawlak, and K. F. Cheung (2007), ADCP observations of edge waves off Oahu in the wake of the November 2006 Kuril Islands Tsunami, *Geophys. Res. Lett.*, *34*, L23617, doi:10.1029/2007GL032015.

Eich, M. L., M. A. Merrifield, and M. H. Alford (2004), Structure and variability of semidiurnal internal tides in Mamala Bay, Hawaii, *J. Geophys. Res.*, *109*, C05010, doi:10.1029/2003JC002049.

Emery, W. J., and R. E. Thompson (2001), *Data Analysis Methods in Physical Oceanography*, 2nd ed., 638 pp. Elsevier, Amsterdam.

Grilli, S. T., J. C. Harris, T. Tajalibakhsh, T. L. Masterlark, C. Kyriakopoulus, J. T. Kirby, and F. Shi (2013), Numerical simulation of the 2011 Tohoku tsunami based on a new transient FEM co-seismic source: Comparison to far- and near-field observations, *Pure Appl. Geophys.*, *170*(6–8), 1333–1359.

González, F. I., K. Satake, E. F. Boss, and H. O. Mofjeld (1995), Edge wave and non-trapped modes of the 25 April 1992 Cape Mendocino tsunami, *Pure Appl. Geophys.*, *144*(3–4), 409–426.

Horrillo, J., W. Knight, and Z. Kowalik (2008), Kuril Islands tsunami of November 2006: 2. Impact at Crescent City by local enhancement, *J. Geophys. Res.*, *113*, C01021, doi:10.1029/2007JC004404.

Ito, Y., T. Tsuji, Y. Osada, M. Kido, D. Inazu, Y. Hayashi, H. Tsushima, R. Hino, and H. Fujimoto (2011), Frontal wedge deformation near the source region of the 2011 Tohoku-Oki earthquake, *Geophys. Res. Lett.*, *38*, L00G05, doi:10.1029/2011GL048355.

Johnson, A. E., B. S. Powell, and G. F. Steward (2013), Characterizing the effluence near Waikiki, Hawaii with a coupled biophysical model, *Cont. Shelf Res.*, *54*, 1–13.

Lacy, J. R., D. M. Rubin, and D. Buscombe (2012), Currents, drag, and sediment transport induced by a tsunami, *J. Geophys. Res.*, *117*, C09028, doi:10.1029/2012JC007954.

Lay, T., C. J., Ammon, H. Kanamori, L. Xue, and M. J. Kim (2011), Possible large near-trench slip during the great 2011 Tohoku (Mw 9.0) earthquake, *Earth Planets Space*, *63*(7), 687–692.

Lowe, R. J., J. L. Falter, S. G. Monismith, and M. J. Atkinson (2009), Wave-driven circulation of a coastal reef-lagoon system, *J. Phys. Oceanogr.*, *39*(4), 873–893.

Lynett, P., R. Weiss, W. Renteria, G. D. L. T. Morales, S. Son., M. E. M. Arcos, and B. T. MacInnes (2013), Coastal impacts of the March 11th Tohoku, Japan tsunami in the Galapagos Islands, *Pure Appl. Geophys.*, *170*(6–8), 1189–1206.

Mori, N., T. Takahashi, T. Yasuda, and H. Yanagisawa (2011), Survey of 2011 Tohoku earthquake tsunami inundation and run-up, *Geophys. Res. Lett.*, *38*, L00G14, doi:10.1029/2011GL049210.

Munger, S., and K. F. Cheung (2008), Resonance in Hawaii waters from the 2006 Kuril Islands Tsunami, *Geophys. Res. Lett.*, *35*, L07605, doi:10.1029/2007GL032843.

Okada, Y. (1985), Surface deformation due to shear and tensile faults in a half space, *Bull. Seismol. Soc. Am.*, *75*(4), 1135–1154.

Roeber, V., and K. F. Cheung (2012), Boussinesq-type model for energetic breaking waves in fringing reef environment, *Coastal Eng.*, *70*, 1–20.

Roeber, V., K. F. Cheung, and M. H. Kobayashi (2010a), Shock-capturing Boussinesq-type model for nearshore wave processes, *Coastal Eng.*, *57*(4), 407–423.

Roeber, V., Y. Yamazaki, and K. F. Cheung (2010b), Resonance and impact of the 2009 Samoa tsunami around Tutuila, American Samoa, *Geophys. Res. Lett.*, *37*(21), L21604, doi:10.1029/2010GL044419.

Simons, M., et al. (2011), The 2011 magnitude 9.0 Tohoku-oki earthquake: Mosaicking the megathrust from seconds to centuries, *Science*, *332*(6036), 1421–1425.

Sobarzo, M., J. Garcés-Vargas, L. Bravo, A. Tassara, and R. A. Quiñones (2012), Observing sea level and current anomalies driven by a megathrust slope-shelf tsunami: The event on February 27, 2010 in central Chile, *Cont. Shelf Res.*, *49*, 44–55.

Tsai, V. C., J. Ampuero, H. Kanamori, and D. J. Stevenson (2013), Estimating the effect of Earth elasticity and variable water density on tsunami speeds, *Geophys. Res. Lett.*, *40*, 492–496, doi:10.1002/grl.50147.

Ursell, F. (1952), Edge waves on a sloping beach, *Proc. R. Soc. London, Ser. A*, *214*, 79–97.

Walker, D. (2004), Regional tsunami evacuations for the state of Hawaii: A feasibility study on historical runup data, *Sci. Tsunami Hazards*, *22*, 3–22.

Wei, Y., C. Chamberlin, V. V. Vasily, L. Tang, and E. N. Bernard (2013), Modeling of the 2011 Japan tsunami: Lessons for near-field tsunami forecast, *Pure Appl. Geophys.*, *170*(6–8), 1309–1331.

Wessel, P., and W. H. F. Smith (1991), Free software helps map and display data, *Eos Trans. AGU*, *72*(41), 445–446.

Yamazaki, Y., and K. F. Cheung (2011), Shelf resonance and impact of near-field tsunami generated by the 2010 Chile earthquake, *Geophys. Res. Lett.*, *38*, L12605, doi:10.1029/2011GL047508.

Yamazaki, Y., K. F. Cheung, and Z. Kowalik (2011a), Depth-integrated, non-hydrostatic model with grid nesting for tsunami generation, propagation, and run-up, *Int. J. Numer. Methods Fluids*, *67*(12), 2081–2107.

Yamazaki, Y., K. F. Cheung, and T. Lay (2013), Modeling of the 2011 Tohoku near-field tsunami from finite-fault inversion of seismic waves, *Bull. Seismol. Soc. Am.*, *103*(2b), 1444–1455.

Yamazaki, Y., Z. Kowalik, and K. F. Cheung (2009), Depth-integrated, non-hydrostatic model for wave breaking and runup, *Int. J. Numer. Methods Fluids*, *61*(5), 473–497.

Yamazaki, Y., K. F. Cheung, G. Pawlak, and T. Lay (2012), Surges along the Honolulu coast from the 2011 Tohoku tsunami, *Geophys. Res. Lett.*, *39*, L09604, doi:10.1029/2012GL051624.

Yamazaki, Y., T. Lay, K. F. Cheung, H. Yue, and H. Kanamori (2011b), Modeling near-field tsunami observations to improve finite-fault slip models for the 11 March 2011 Tohoku earthquake, *Geophys. Res. Lett.*, *38*, L00G15, doi:10.1029/2011GL049130.

Zhang, Y. J., R. C. Witter, and G. R. Priest (2011), Tsunami-tide interaction in 1964 Prince William Sound tsunami, *Ocean Modell.*, *40*(3–4), 246–259.